

UCLA

UCLA Electronic Theses and Dissertations

Title

Optical Characterization of InAs/GaAs_{1-x}Sb_x Quantum-Dot Structures

Permalink

<https://escholarship.org/uc/item/6pt6h1xz>

Author

Zhao, Zhangji

Publication Date

2018

Peer reviewed|Thesis/dissertation

UNIVERSITY OF CALIFORNIA

Los Angeles

Optical Characterization of InAs/GaAs_{1-x}Sb_x Quantum-Dot Structures

A thesis submitted in partial satisfaction

of the requirements for the degree Master of Science

in Electrical Engineering

by

Zhangji Zhao

2018

© Copyright by

Zhangji Zhao

2018

ABSTRACT OF THE THESIS

Optical Characterization of InAs/GaAs_{1-x}Sb_x Quantum-Dot Structures

by

Zhangji Zhao

Master of Science in Electrical Engineering

University of California, Los Angeles, 2018

Professor Chee Wei Wong, Chair

InAs quantum-dot structure were grown on GaAs (001) substrate using GaAs_{1-x}Sb_x matrix. The use of GaAs_{1-x}Sb_x for the buffer and cap layers could suppress coalescence between dots effectively and increase the dot density significantly. Also, InAs/GaAs_{1-x}Sb_x QDs show a band alignment transition from type-I to type-II as the Sb concentration increases. In this work, the quantum-dot structure has been studied using power-dependent photoluminescence to determine the band structure. At low Sb concentration (Sb<13%), InAs/GaAs_{1-x}Sb_x maintain the type-I alignment. At high Sb concentration (Sb>13%), InAs/GaAs_{1-x}Sb_x demonstrate a type-II band structure. Time-resolved photoluminescence measurement is performed to study carrier dynamics in the quantum-dot structure at 7K to understand the type-I and type-II transition in more detail.

The thesis of Zhangji Zhao is approved.

Mona Jarrahi

Aydogan Ozcan

Chee Wei Wong, Committee Chair

University of California, Los Angeles

2018

TABLE OF CONTENTS

1. Introduction.....	1
2. Background.....	2
2.1 Self-assembled Quantum Dots Structure.....	2
2.2 Molecular Beam Epitaxy for Quantum Dots Growth.....	4
3. Characterization Techniques.....	8
3.1 Structural Characterization	8
3.2 Optical Characterization	12
4. Effect of Sb Composition of Optical Properties of InAs/ GaAs _{1-x} Sb _x Quantum Dots.....	14
4.1 Introduction to Intermediate Band Solar Cells (IBSCs).....	14
4.2 Experimental Results and Discussions	18
5. Conclusion	28
References.....	29

LIST OF FIGURES

Fig. 1 Schematic representation of three film growth modes under different coverage (θ) regimes: (a) Layer-by-layer growth (Frank-van der Merwe, FM). (b) Layer-plus island growth (Stranski-Krastanov, SK). (c) Island growth (Vollmer- Weber, VW) 3

Fig. 2 Global chemical sensitive g002 dark field TEM images of sample Ref (left). Zoom of a representative QD from each sample (right). 4

Fig. 3 Schematic diagram of a Solid-Source MBE growth chamber 7

Fig. 4 Different stages of layer-by-layer growth by nucleation of 2D islands and the corresponding intensity of the zero-order diffracted RHEED beam..... 7

Fig. 5 Time evolution of RHEED intensity of InAs QD formation on GaAs with corresponding RHEED patterns. (a) Pure GaAs surface in [110] azimuth, (b) 1ML InAs is deposited, (c) after 2ML InAs deposition. 8

Fig. 6 Schematic diagram of AFM 9

Fig. 7 Symmetric (004) XRD patterns for 20 stacked layers of InAs QDs structure embedded in (a) GaNAs, (b) GaAs space layer. 10

Fig. 8 Ray paths in the TEM under imaging and diffraction conditions 12

Fig. 9 (a) Plan-view bright-field TEM image along (100) zone and (b) cross section image of the structure containing InAs QD array in a 10 nm InGaAs QW. 12

Fig. 10 Schematic band diagrams for the photoluminescence processes in a direct gap material (left) and an indirect gap material (right). 14

Fig. 11 Schematic diagram of (a) time-integrated PL and (b) time-resolved PL	15
Fig. 12 (a) Schematic band diagram of IBSC. (b) Efficiency limit versus lowest band gap, of an IBSC, a two-terminal ideal tandem cell, and single band gap cell	17
Fig. 13 AFM image of InAs QDs with GaAs _{1-x} Sb _x buffer layer. (a)-(c): InAs/ GaAs _{1-x} Sb _x with different Sb composition. (d)-(f): InAs/GaAs _{1-x} Sb _x (x=13%) with different thickness of InAs QD layer.	19
Fig. 14 (a) Schematic diagrams of InAs QD and GaAs/GaAsSb QW structures. (b) PL spectra for corresponding structures.	20
Fig. 15 (a) Schematic diagrams of InAs/GaAsSb QDs samples with Sb=0%, 8%, 11%, 15%, 25% and GaAs/GaAsSb QWs as reference. (b) Normalized PL spectra for corresponding structures. ...	21
Fig. 16 Schematic diagram of band structures. (a) InAs/GaAs QDs. (b) GaAs/GaAsSb QW. (c) InAs/ GaAs _{1-x} Sb _x when x<0.13. (d) InAs/ GaAs _{1-x} Sb _x when x>0.13.	22
Fig. 17 Power-dependent PL at 7K from (a) InAs/GaAs QDs, (b) GaAs/GaAsSb QWs, and (c) InAs/GaAs _{1-x} Sb _x QDs with x=0.11.....	23
Fig. 18 (a) Power-dependent PL at 7K from GaAs _{1-x} Sb _x QDs with x=0.25, the inset shows the linear relationship between the peak (1) energy versus the cube root of excitation energy. (b) PL peak energy versus the cube root of the excitation energy for peak (3) and (2).....	24
Fig. 19 TRPL decay curves measured at 7K for (a) InAs/GaAs QDs, (b) GaAs/GaAsSb QWs, (c) InAs/ GaAs _{1-x} Sb _x QDs with Sb=15% and (d) Sb=25%.....	25

LIST OF TABLES

Table. 1 Nominal compositions and growth rates of the capping layers for the MQD samples.

.....4

ACKNOWLEDGEMENT

First, I would like to express my sincere gratitude to my supervisory committee chair Professor Chee Wei Wong for his generous help for my master's study. It is him who support me to do the research I want and showed me how to be a good researcher. Also, I would like to thank Professor Huffaker for providing this good project.

Second, I would like to thank Doctor Baolai Liang for his direct guidance in my project. His knowledge and experiences greatly helped me during the experiment.

Third, I would also like to thank Bor-Chau Juang, Hyunseok Kim and Dingkun Ren. They warmly welcome me to the lab and gave me a lot of help. Meanwhile, I would like to thank all the friends here in UCLA. Their company made my life colorful.

In the end, I would like to greatly thank my parents and my girlfriend. Nothing would happen without their unconditional support.

1. Introduction

Solar cells (SCs) have been widely studied as one of the most promising clean power sources. The single junction solar cell is predicted to have a theoretical maximum efficiency of 31% by Shockley and Queisser [1]. Thermalization and energy lower than the band gap are two main reasons for the energy loss of Shockley Queisser limit. Several approaches have been proposed to exceed the limit, such as SCs with multiple exciton generation [2], hot carrier SCs [3], multi-junction SCs [4] and intermediate band solar cells (IBSCs). The last one of these is considered as the most promising type and the concept has been firstly described by Luque and Martí in 1997, greatly improved the theoretical maximum conversion efficiency to 63.2% [5]. To put this structure into practice, self-assembled quantum dots (SAQDs) structure has been investigated due to its strong quantum confinement. However, the record of the QDs solar cell has reached is lower than 10% [6], even far away from Shockley Queisser limit. One of the greatest issue is to reduce the strain accumulation, which causes the crystal dislocation and the quality of quantum dots. As we know, strain between different layers mainly results from the lattice mismatch and less strain can be achieved by applying strain compensation layers. Meanwhile, the energy band alignment can be modified under the effect of spacer. In this work, capping InAs/GaAs QDs with $\text{GaAs}_{1-x}\text{Sb}_x$ layer has been studied by varying the composition of Sb. The fundamental concept of solar cell and SAQDs are briefly reviewed. Molecular beam epitaxy technique used to deposition the quantum dot structure is reviewed also. Later, structural and optical characterization methods are discussed, including AFM, XRD, TEM, time-integrated PL and TRPL. The experimental results are presented at last.

2. Background

a) Self-assembled Quantum Dots Structure

The self-assemble structure is based on the formation of coherently strained islands and 2D to 3D growth transition controlling which is induced by a misfit strain in the epitaxial structure. For thin film epitaxial growth, there are three primary modes, including layer by layer growth, layer plus island growth and island growth, as illustrated in the Fig. 1 [7]. Layer by layer growth is also called as Frank-van der Merve (F-M) mode. The interaction force between the substrate and layer is stronger than neighboring layers, and thus each new layer would not start growing until the last layer finished. The counter case is characterized as the island growth, called Vollmer-Weber (V-W) mode. Its interaction between the substrate and layer is weaker, leading to the formation of three-dimensional islands. The intermediate case is known as Stransky-Krastanov (S-K) mode, characterized as the layer-plus-island growth mode. After one or several layers complete, isolated islands formation starts, to reduce the surface energy.

Self-assembled Quantum Dots (QDs) are grown under the strain relaxation process in epitaxial system using S-K growth method. The main benefit of S-K mode is the uniform size distribution when compared with V-M mode [34]. The deposited material would have a much larger lattice constant than the underlying layer material to accumulate the strain at initial growth. Take InAs dots on GaAs as an example, the lattice mismatch is 7.2%. At initial stage, a few monolayers of InAs is formed on the GaAs surface, called wetting layer (WL). The in-plane lattice mismatch would induce strain to the WL layer compressively while the GaAs layer is tensile strained. As the InAs coverage increases to 1.75 monolayer, the strain energy is reduced by elastic energy relaxation due to the 3D island formation [8].

Capping process is a key factor responsible for the stability of quantum dots. It also changes the morphology of QDs significantly due to the strain and intermixing. An example is shown in Fig.2, the transmission electron microscopy (TEM) images of InAs QDs capped by different capping layers (CLs) with composition of GaAs(Sb)(N), which are listed in table 1. The QDs, the wetting layer (WL) with a darker contrast with respect to GaAs, and the CL can be clearly distinguished in the images [9].

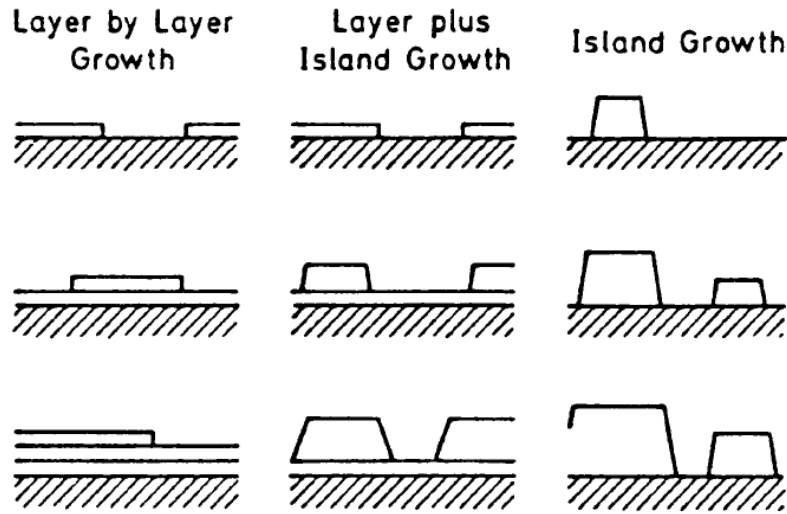


Fig. 1 Schematic representation of three film growth modes under different coverage (θ) regimes: (a) Layer-by-layer growth (Frank-van der Merwe, FM). (b) Layer-plus island growth (Stranski-Krastanov, SK). (c) Island growth (Vollmer-Weber, VW) [7]

Sample	%Sb in the CL	%N in the CL	CL growth rate (ML/s)
Ref	0	0	1
GaAsSb10	10	0	2
GaAsSb20	20	0	1
GaAsN	0	2	2
GaAsSbN	10	2	2
GaAsSbN-SL	10	2	1
GaAsSbN-thin	20	4	1

Table. 1 Nominal compositions and growth rates of the capping layers for the MQD samples. [9]

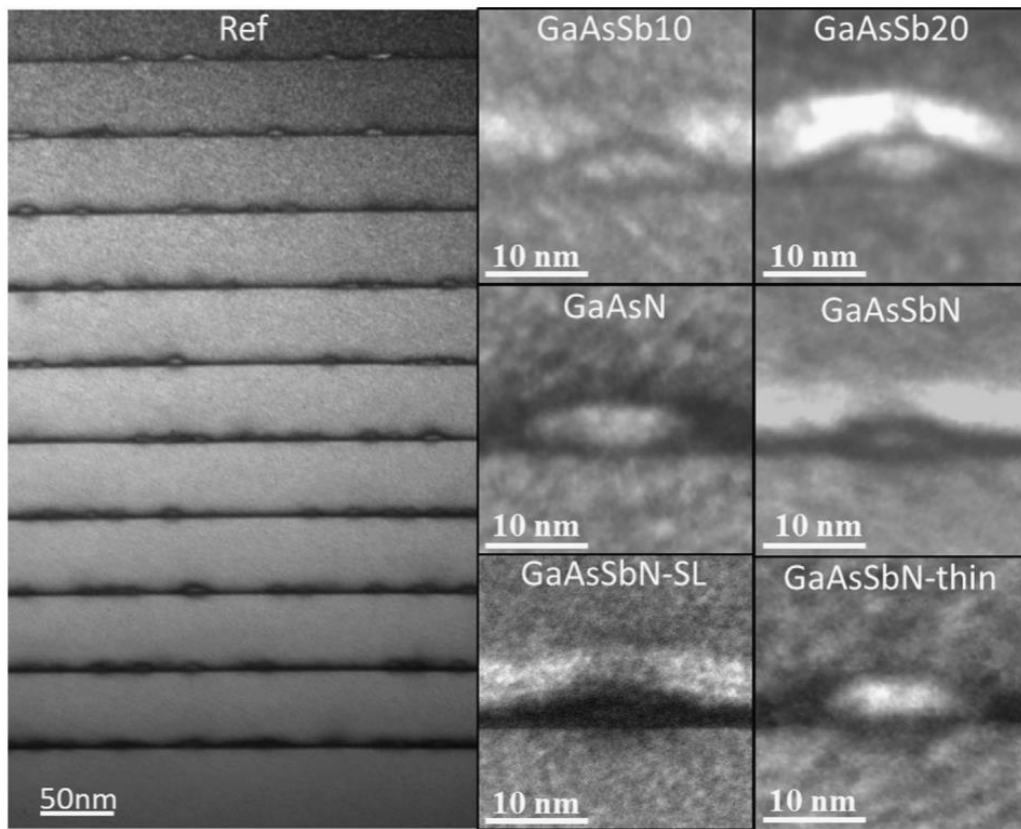


Fig. 2 Global chemical sensitive g002 dark field TEM images of sample Ref (left). Zoom of a representative QD from each sample (right). [9]

b) Molecular Beam Epitaxy for Quantum Dots Growth

Molecular Beam Epitaxy (MBE) is an epitaxial growth technique for thin-film deposition with great precision and purity, based on the interaction of atoms and molecules beams of thermal energy on a heated surface under ultra-high vacuum (UHV) conditions [10]. It allows the growth of different nanostructures such as quantum well, quantum dots and quantum wires. Different types of MBE are developed for various materials, such as Gas-Source MBE (GSMBE), Metalorganic MBE (MO-MBE) and Solid-Source MBE (SS-MBE). For the case of group-III and -V nanostructure, the Solid-Source MBE is used to produce the molecular beams by the effusion cells and the beams are impinged on the rotating substrate in a growth chamber [11]. The main components of a Solid-Source MBE system are shown in Fig. 3. Many in-situ analysis tools are available in the growth chamber or can be connected to the chamber, to characterize the growth process, such as Reflection High Energy Electron Diffraction (RHEED) to study the growing surface, Auger Electron Spectroscopy (AES), X-ray Photoelectron Spectroscopy (XPS) and Secondary Ion Mass Spectroscopy (SIMS).

The UHV condition is required to reduce partial pressure of impurities during growth process. Also, it helps the molecular beams to impinge unreacted area of substrate surface by increasing their mean free path. To reach 10^{-11} Torr growth environment, the chamber is equipped with liquid-nitrogen shrouds and connected with several pumps such as ion pump, turbo pump, titanium sublimation pump and cryogenic pump.

To concluded the growth process, electron beam is generated by an electron gun with an energy ~ 10 keV. The beam is collimated and impinges onto the substrate with a glancing angle ($\sim 1-3^\circ$). The diffracted electrons hit the fluorescent screen and create a diffraction pattern, allowing the real-time study of the growing surface. Based on the analysis of the Ewald

construction on a reciprocal two-dimensional (2D) lattice [11], the streaky feature is from the diffraction of an atomically flat surface and shows up few tens of seconds of the growth.

RHEED could provide the information of the surface roughness, surface reconstruction and the time dependence of the intensity of diffracted streaks. The electrons only penetrate the first few monolayers of the material due to the glancing incidence which makes RHEED highly surface sensitive. As shown in Fig. 4, the intensity of the zero-order diffracted beam exhibits a damped oscillation pattern as the growth starts. When the deposition coverage $\theta = 0$ ML, the reflection intensity has its maximum. As the deposition coverage θ increases from 0 ML to 0.5 ML, the increased surface roughness reduces the reflection intensity. As the coverage θ increases from 0.5 ML to 1 ML, the decreased roughness recovers the reflection intensity.

A typical RHEED pattern is shown in Fig. 5, which describes the formation process of InAs quantum dots grown on GaAs surface. The RHEED patterns at different stages are corresponding with their intensities. At the beginning, the RHEED pattern is from the diffraction of the two-dimensional surface. As the coverage θ surpasses the critical value θ_c , the RHEED pattern changes qualitatively, shows three-dimensional diffraction pattern [12].

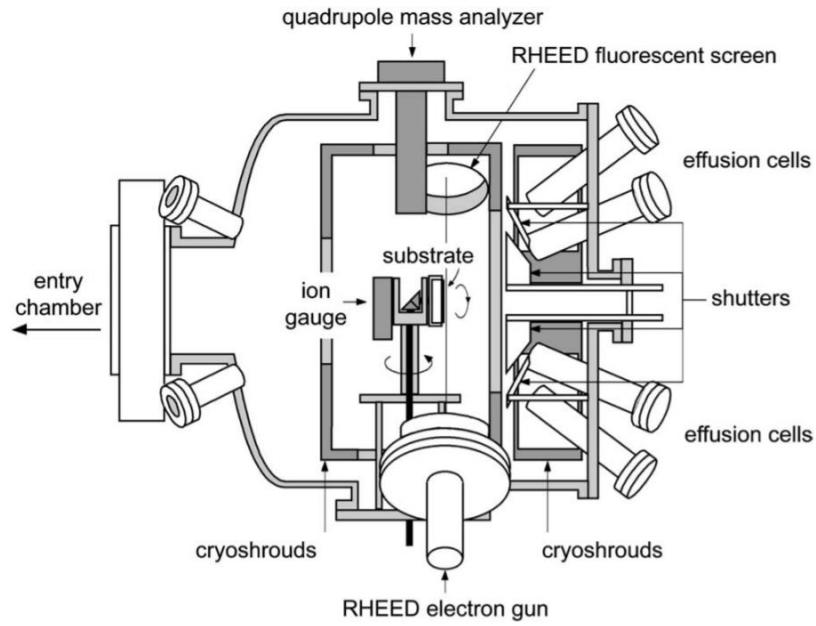


Fig. 3 Schematic diagram of a Solid-Source MBE growth chamber. [10]

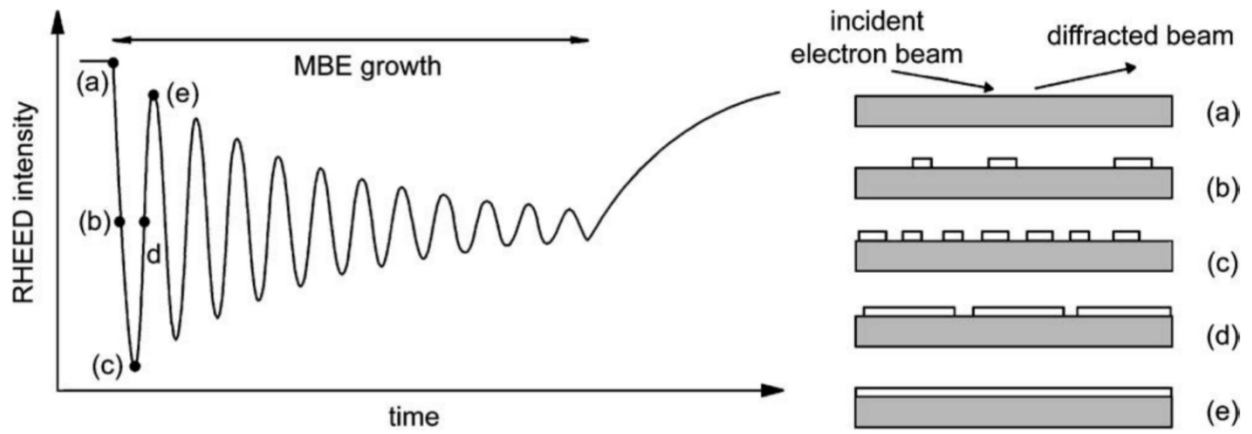


Fig. 4 Different stages of layer-by-layer growth by nucleation of 2D islands and the corresponding intensity of the zero-order diffracted RHEED beam. [7]

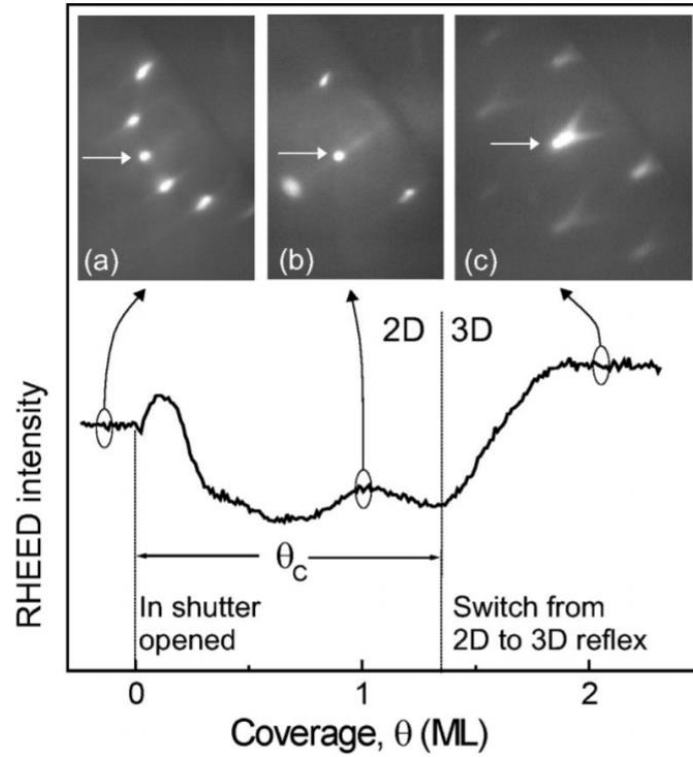


Fig. 5 Time evolution of RHEED intensity of InAs QD formation on GaAs with corresponding RHEED patterns. (a) Pure GaAs surface in [110] azimuth, correspond with a 2D-type diffraction, (b) 1ML InAs is deposited, with 2D-type diffraction, (c) after 2ML InAs deposition, shows a 3D-type diffraction [12].

3. Characterization Techniques

a) Structural Characterization

AFM

Atomic force microscopy (AFM) is a type of scanning force microscopy (SFM), which can provide a resolution on the order of fractions of a nanometer. It has been widely applied on force measurement, imaging, and manipulation. For morphological characterization of nanostructures, the atomic interaction of surface will bend the cantilever when its tip close to the surface [19]. Based on the configuration of AFM in Fig. 6, the photodiode detects deflection of the cantilever with high precision. The distance between sample and tip is calibrated by the feedback loop, to maintain a constant phase and frequency. The piezoelectric scanner controls sample position and signals would be processed to generate AFM images. The surface can be mapped by three modes: contact mode, non-contact mode and tapping mode. The contact mode has a high mapping resolution, but the sample will be damaged as the tip would touch the surface. In non-contact mode, the sample will not be damaged due the Van der Waals forces between tip and sample, but the resolution is lower. In tapping mode, the tip oscillates vertically at the frequency of 50 to 500 kHz. The oscillation amplitude is reduced as the tip touches the surface and it would not damage the surface. Tapping mode is used for SAQDs to acquire the quantum dot density, height and morphology.

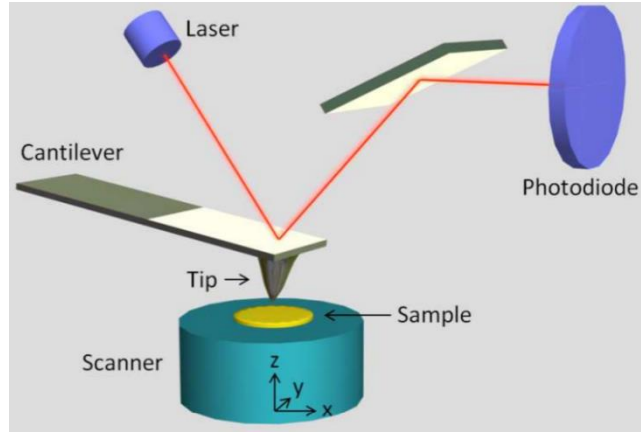


Fig. 6 Schematic diagram of AFM. [19]

XRD

X-ray diffraction (XRD) has been widely used to study crystal lattice constant and geometry, materials identification, orientation of crystals and etc. It is based on Bragg's law, which described by the relation between the diffraction angle and interplanar spacing of crystal.

$$\lambda = 2d \sin \theta, \quad d = \frac{a_0}{\sqrt{l^2 + k^2 + h^2}}$$

where λ is the wavelength of x-ray, d is the interplanar spacing for cubic crystal, θ is the diffraction angle, a_0 is the crystal lattice constant, h , k and l are the Miller indices of the Bragg plane.

An example of XRD spectra is shown in Figure. 7 for InAs QDs grown on GaNAs and GaAs substrate. The satellite peaks originating from the periodic superlattice structure can be clearly observed in each sample. The zeroth-order satellite peak $S(0)$ of InAs/GaNAs sample shows a close lattice with GaAs substrate [20].

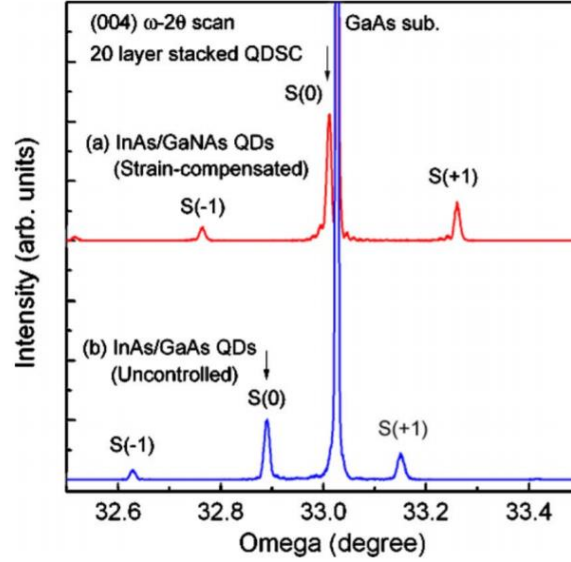


Fig. 7 Symmetric (004) XRD patterns for 20 stacked layers of InAs QDs structure embedded in (a) GaNAs, (b) GaAs space layer. S(x) means xth-order satellite peak. [20]

TEM

TEM (transmission electron microscopy) makes use of electron beams to transmit through thin enough specimens to obtain the structural information. There are two different modes as illustrated in the Fig. 8. Under image mode, the electrons are scattered by the specimen and the rest hit the screen to form the image. The high magnification of TEM results from the small electron wavelength. According to the de Broglie relationship,

$$\lambda = \frac{h}{\sqrt{2mqV\left(\frac{qV+1}{2mc^2}\right)}}$$

where h is the Planck constant, m and q are the electron mass and charge. V is the accelerating voltage. An example of TEM image of InAs QDs in InGaAs QWs is shown in Fig. 9. The size, height and the distribution of InAs QDs can be clearly distinguished.

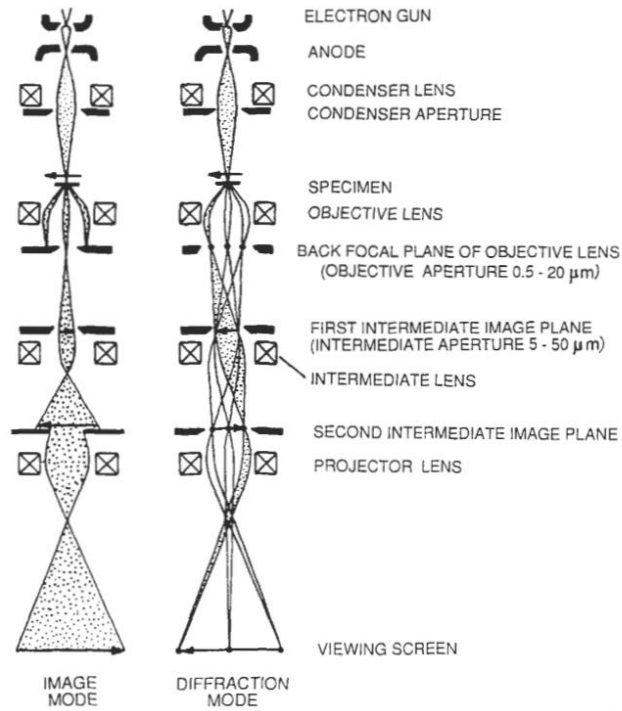


Fig. 8 Ray paths in the TEM under imaging and diffraction conditions [7].

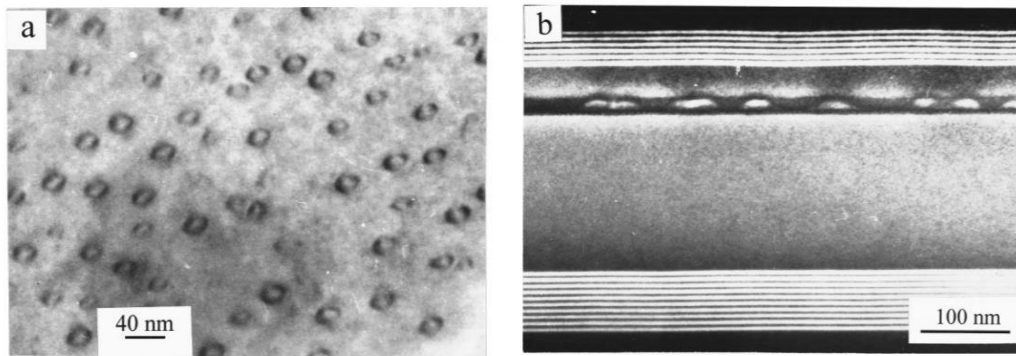


Fig. 9 (a) Plan-view bright-field TEM image along (100) zone and (b) cross section image of the structure containing InAs QD array in a 10 nm InGaAs QW [7].

b) Optical Characterization

Photoluminescence (PL)

Photoluminescence (PL) is a powerful optical spectroscopy method, which can be used to identify the impurities, determine the band gap and activation energy of semiconductor structures. The fundamental process is the spontaneous emission of photons when a semiconductor is pumped by a light source that has higher energy than its band gap. The PL process for direct band gap and indirect band gap is illustrated by the E-k diagram in Fig. 10. Shortly after electrons and holes are excited to their initial excited states, the electron-hole pairs recombine radiatively with the emission of a photon, which is the PL process. When the conduction band (CB) minimum and valence band (VB) maximum of a semiconductor both located at $k=0$, it is characterized as direct band gap material. When the CB minimum does not occur at $k=0$ as VB does, the material has an indirect band gap. The energy and momentum conserve for both the photon absorption and photoluminescence processes. For direct band gap structure, since the CB minimum and VB maximum have the same wave vector k , there are no phonon get involved. In contrast, CB minimum and VB maximum have different k value in indirect band gap material, which means the photon absorption and emitting process need to be assisted by phonon, to conserve the momentum. Apparently, PL in direct band gap material has a much higher efficiency.

PL spectroscopy is a very effective and nondestructive measurement method for QD structure characterization and the inter-band optical transition can be studied by time-integrated PL. Fig. 11 (a) shows a schematic diagram of a time-integrated PL setup. The sample mounted in the cryostat is excited laser, which is chopped to high frequency to increase signal-to-noise ratio. The photons of PL are focus into a monochromator and split into various wavelengths by the

grating. The photodiode converts photons into electrical signal and amplified by a lock-in amplifier and collected by the computer.

It is a very rapid process of electron-hole pairs relaxation and recombination. PL in direct band gap structure is a first-order process with a much shorter radiative lifetime ($\sim 10^{-8}$ s), comparing with the lifetime ($\sim 10^{-4}$ s) in indirect band gap, which is a second-order process because of involvement of phonons. To study the carrier dynamics, time-resolved PL (TRPL) measurement based on a time-correlated single photon counting (TCSPC) system can be used to detect the lifetime of carriers. As shown in Fig. 11 (b), the correlator is triggered by the pulsed laser to start to measure the signal and the decay time of the carrier can be displayed on the computer.

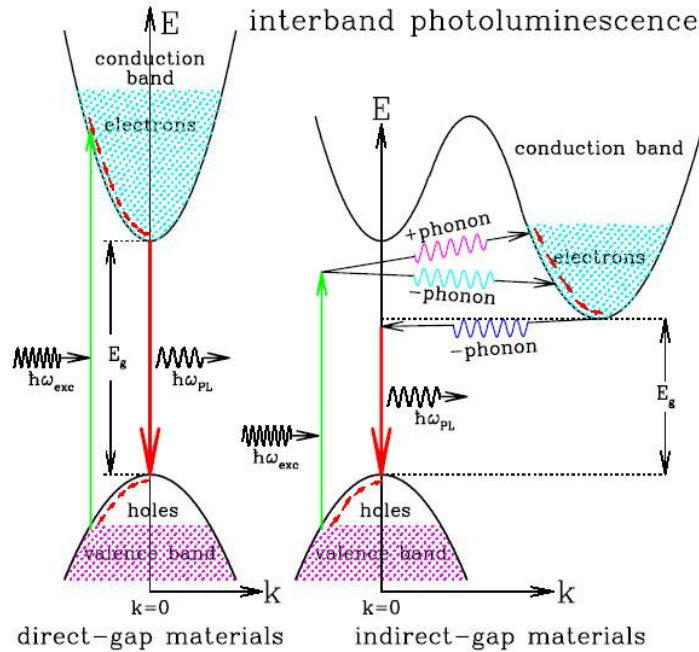


Fig. 10 Schematic band diagrams for the photoluminescence processes in a direct gap material (left) and an indirect gap material (right). The shaded states at the bottom of the CB and the empty states at the top of the VB represent the electrons and holes created respectively by the absorption of photons with energy higher than the band gap (E_g). Phonon assist absorption and photoluminescence processes are illustrated in indirect-gap material. [22]

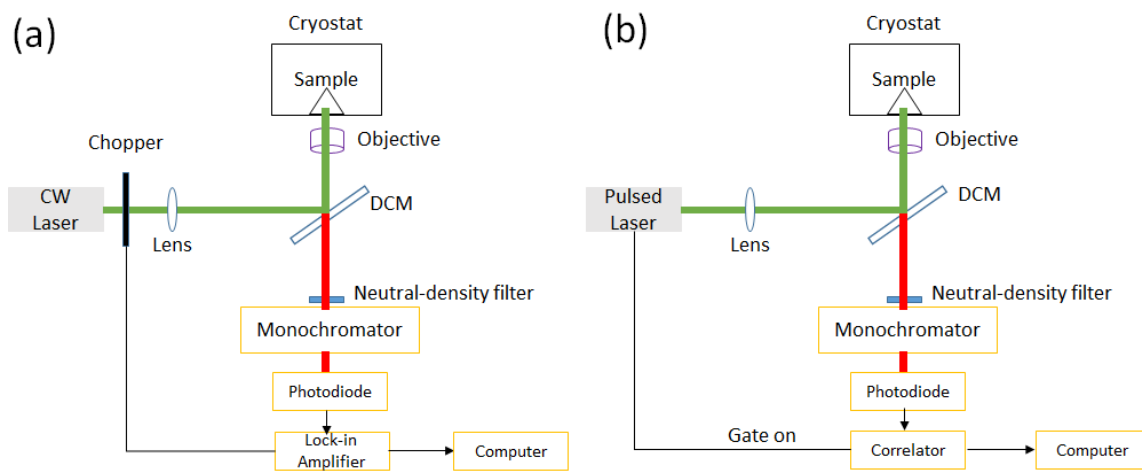


Fig. 11 shows the schematic diagram of (a) time-integrated PL and (b) time-resolved PL.

4. Effect of Sb Composition of Optical Properties of InAs/ GaAs_{1-x}Sb_x Quantum Dots

4.1 Introduction to Intermediate Band Solar Cells (IBSCs)

For conventional solar cells, the fundamental principle is that one electron would be excited from the valence band (VB) to conduction band (CB) by a single photon, creating electron-hole pairs, thus generating electrical current under the effect of pn-junction through external load. To form the pn-junction, the semiconductor would be doped by impurities.

The intermediate band solar cell (IBSC) has been proposed to make use of photons less than the bandgap energy. The conceptual diagram of IBSC is presented in Fig. 12(a), and its maximum efficiency is compared with a two-terminal ideal tandem cell and a single band gap in Fig. 12(b), where the IBSC exhibits a higher maximum efficiency over the other two structures [5]. The IBSC is characterized by the existence of an energy band of states inside the bandgap between the CB and the VB. In this way, photons with energy less than the bandgap can be absorbed to pump electrons, allowing two sub-bandgap carrier transitions, from VB to IB and from IB to CB. Thus, solar cell current can be increased without output voltage degradation.

Self-assembled quantum dots (SAQDs) structure has been proposed for taking IBSC into practice but several difficulties follows. First, the QD states require a quasi-Fermi level that separated from the Fermi level of the bulk to avoid reduction of the open-circuit voltage (V_{oc}), which determined by the host material band gap [12]. However, during the SK growth process, strain would accumulate in the crystal and degrade the vertically aligned QD structure, which harms the effective energy band gap of host material. Much effort has been attempted to reduce strain between host material and QD layers by inserting strain compensation layers. For example, GaP layers has been shown to be effectively reduce strain between InAs/GaAs SAQDs [14].

However, as the open-circuit voltage still badly degraded, the conversion efficiency of the SAQDs with GaP layers remains lower than a baseline cell which without QDs.

Recently, GaAsSb layer has been experimentally proved to be a feasible strain compensation layer on InAs QDs [15], which could enhance the thermal stability, the crystal and QDs quality [16]. It provides a better device performance and suppresses the non-radiative recombination. What's more, the type-II band alignment of InAs/GaAs SAQDs with GaAsSb layer shows a longer the carrier lifetime comparing with the type I band arrangement of the QDs structure without GaAsSb layer [17]. It has been reported that Sb start to exhibit the type-II behavior when the Sb composition reached 14% [18].

The strain compensation layers such as GaAs, GaSb, AlAsSb and GaAsSb have been used as both buffer and cap layers in InAs QD structure. In this work, GaAs_{1-x}Sb_x is capped onto the InAs QD layer and the effect of Sb composition is studied.

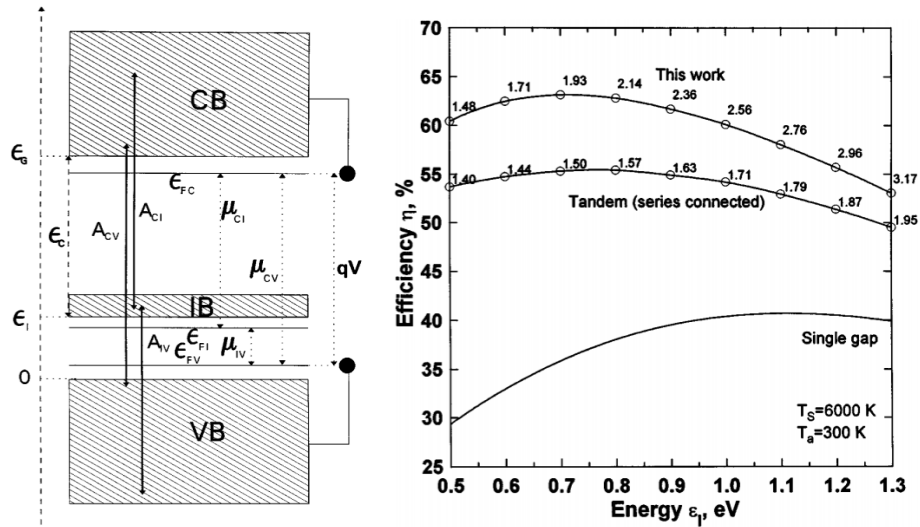


Fig. 12 (a) Schematic band diagram of IBSC. (b) Efficiency limit versus lowest band gap, of an IBSC, a two-terminal ideal tandem cell, and single band gap cell. [5]

4.2 Experimental Results and Discussions

All samples are grown by Solid-Source MBE reactor on semi-insulating GaAs (100) substrates. A 100nm GaAs buffer layer is deposited on a semi-insulating GaAs (100) at 580 °C after native oxidation layer thermally removal. The substrate is ramped down to 505 °C for the growth of InAs layer with different thickness and the growth rate is 0.1 ML/s under an As₂/In beam equivalent pressure (BEP) ratio between 25 and 35. The 10 nm GaAs_{1-x}Sb_x layer is capped onto the InAs QD layer, with the composition of Sb varies from 0% to 25%. After this, a GaAs capping layer completes the growth.

a. QDs quality evaluated by AFM

In order to study the effect of how the GaAs_{1-x}Sb_x layer affects the InAs QDs, uncapped InAs QD layers are grown on GaAs_{1-x}Sb_x buffer layer. Fig. 13 shows two sets of QDs samples. InAs QDs samples have different Sb composition with same thickness of 3ML are present in Fig. 13 (a)-(c). The lower and higher Sb composition is Fig. 13 (a) and (c) are showing that some QDs coalescence respectively. And Fig. 13 (b) shows the best quality of QDs with Sb=13%. With same composition of Sb=13%, InAs QDs with thickness of 2ML, 3ML and 3.5ML are present in Fig. 13 (d)-(f). The areal density increases from 6.5×10^{10} to $3.5 \times 10^{11}/cm^2$ as the InAs thickness increases from 2ML to 3ML. The QD density drops when the thickness increases to 3.5ML. The highest QD density is achieved at 3ML of InAs QD layer and it is mainly because of the effective suppression of coalescence between dots [23]. Previous study has been shown to illustrate that the buffer layer induced strain would quench the interaction between QDs, and thus affect the uniformity. [24]

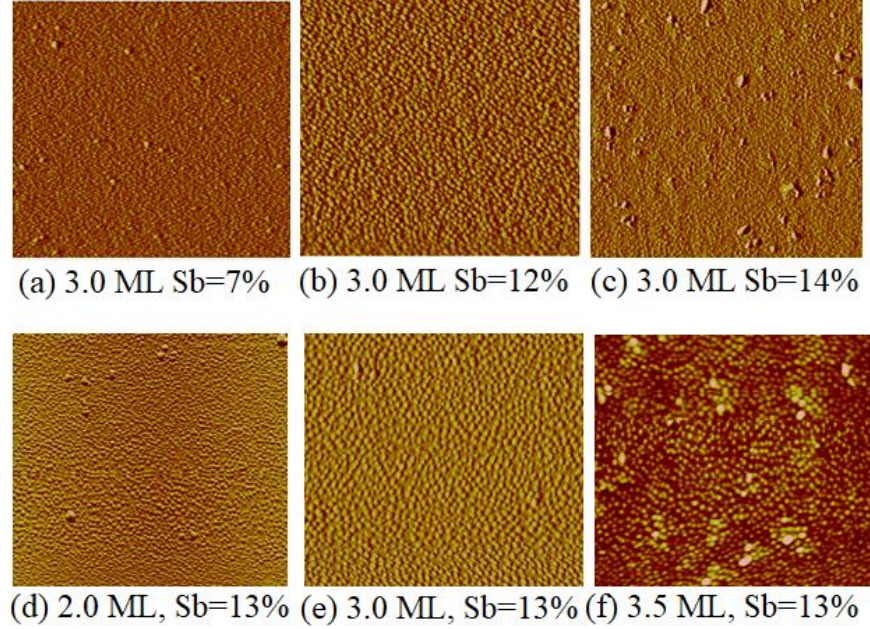


Fig. 13 AFM image of InAs QDs with $\text{GaAs}_{1-x}\text{Sb}_x$ buffer layer. (a)-(c): InAs/ $\text{GaAs}_{1-x}\text{Sb}_x$ with different Sb composition. (d)-(f): InAs/ $\text{GaAs}_{1-x}\text{Sb}_x$ ($x=13\%$) with different thickness of InAs QD layer.

b. Optical characterization by PL

In order to have a more detailed knowledge of the InAs QD structure and GaAs/GaAsSb quantum well (QW) structure, a set of samples shown in Fig. 14 (a) are grown to set as references. Low temperature (7K) PL measurements are performed with a 532 nm continuous-wave laser. We can determine the PL peak positions and relative intensities for the samples of InAs/GaAs QDs, GaAs/GaAsSb QWs, GaAsSb bulk and InAs/GaAsSb QDs, as shown in Fig. 14 (b). Under same excitation, the InAs/GaAs QD structure shows the strongest PL intensity with two layers of QD, indicates a higher PL efficiency comparing with QW structure. Also, the 8 stacked GaAs/GaAsSb QW shows a higher PL intensity than the single heterostructure, indicates the multistack structure can effectively enhance the optical property without changing the emission wavelength. The PL peak is redshifted by adding the GaAsSb layer onto the QD layer, which shows the emission wavelength can be tuned by changing Sb composition.

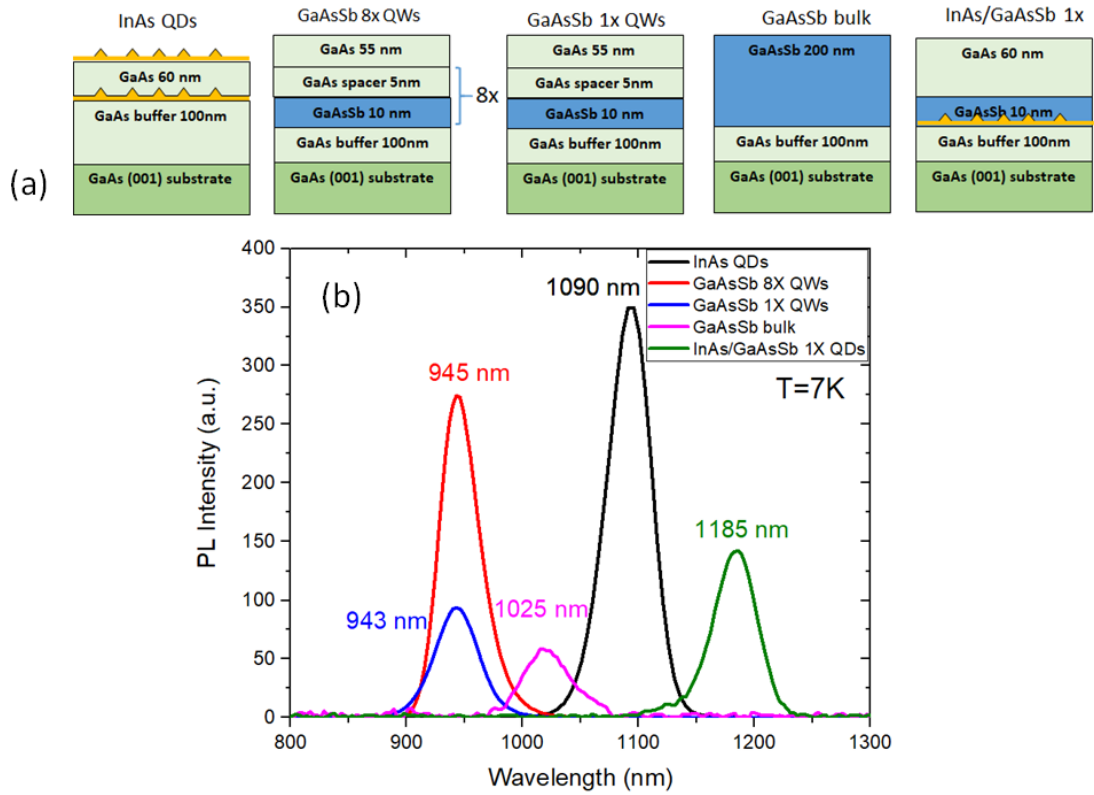


Fig. 14 (a) Schematic diagrams of InAs QD and GaAs/GaAsSb QW structures. (b) PL spectra for corresponding structures.

Another set of samples are prepared to study the optical properties of InAs/ GaAs_{1-x}Sb_x QDs under different Sb compositions, as illustrated in Fig. 15 (a). PL spectra are measured under low temperature (7K) with a low excitation intensity of 0.1mW, as shown in Fig. 15 (b). As the concentration of Sb increases, from 0% to 8% and 11%, the PL peaks are redshifted from 1113 nm to 1182 nm and 1230 nm respectively, and the full-width at half-maximum (FWHM) decreases. The narrower FWHM indicates a better uniformity and carrier confinement of the InAs QDs. At low Sb concentration, the GaAs_{1-x}Sb_x layer acts mainly as a strain compensation layer, which enhances the QDs qualities by reducing the strain. As the Sb composition increases to 15% and 25%, previous studies have shown that the spectra broadening is not only contributed to the

reduced strain and type I to type II transition, but also due to the strain field of the QDs results from the inhomogeneous Sb accumulation on top of the QDs [25-27]. Also, the peaks are redshifted by 237 nm and 192 nm from Sb=0% to 15% and 25% correspondingly. This large redshift mainly originates from the QDs reshape and band structure change [28]. The QDs height would increase as the Sb accumulation on top of the dot, which prevents the QD from decomposing. The band alignment is modified by the GaAsSb spacer at high Sb concentration.

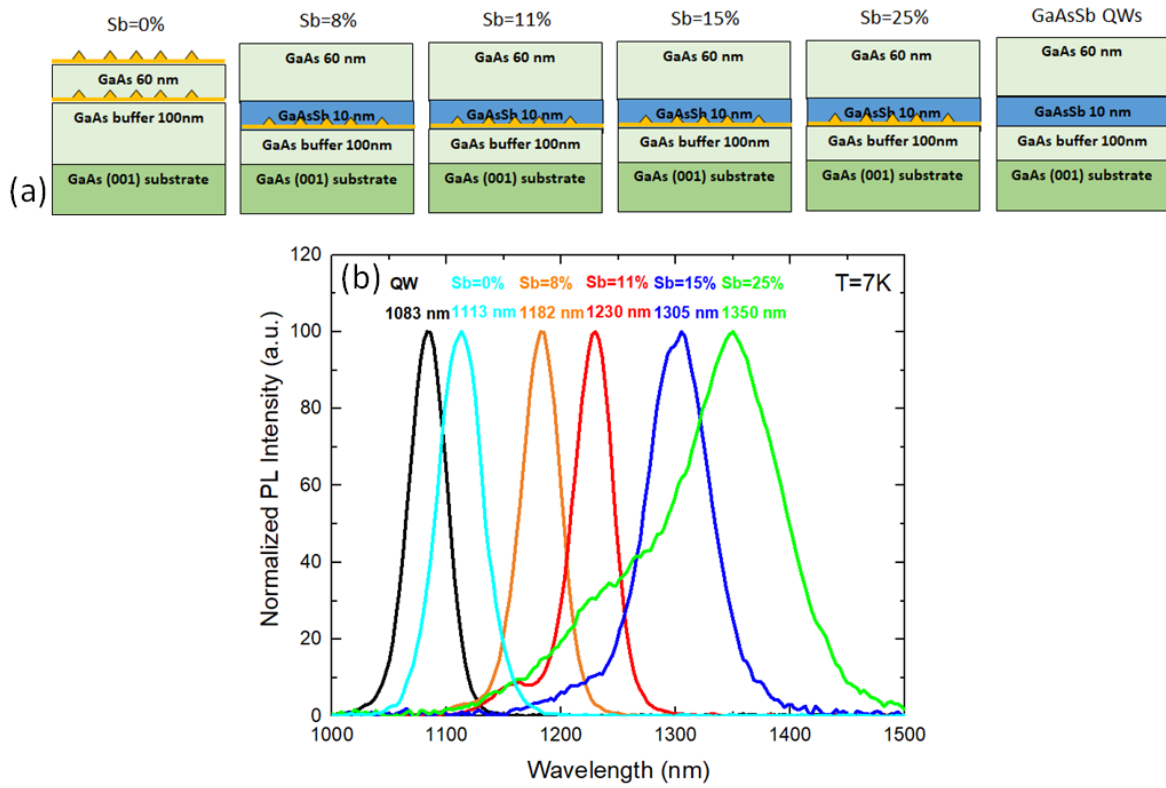


Fig. 15 (a) Schematic diagrams of InAs/GaAsSb QDs samples with Sb=0%, 8%, 11%, 15%, 25% and GaAs/GaAsSb QWs as reference. (b) Normalized PL spectra for corresponding structures.

In order to understand the band alignment evolution along with the Sb concentration, the schematic diagrams of energy band structures are shown in Fig. 16. The type-I band alignment of InAs/GaAs QDs and the type-II band alignment of GaAs/GaAsSb are depicted in Fig. 16 (a) and (b). For InAs/ GaAs_{1-x}Sb_x structure, the valence band of the GaAs_{1-x}Sb_x layer rises with the higher

Sb composition. When Sb composition exceeded the critical point (Sb~13%), the valence band of $\text{GaAs}_{1-x}\text{Sb}_x$ will be higher than the valence band of QDs, shows a band alignment transition from type-I to type-II as illustrated in Fig. 16 (c) and (d).

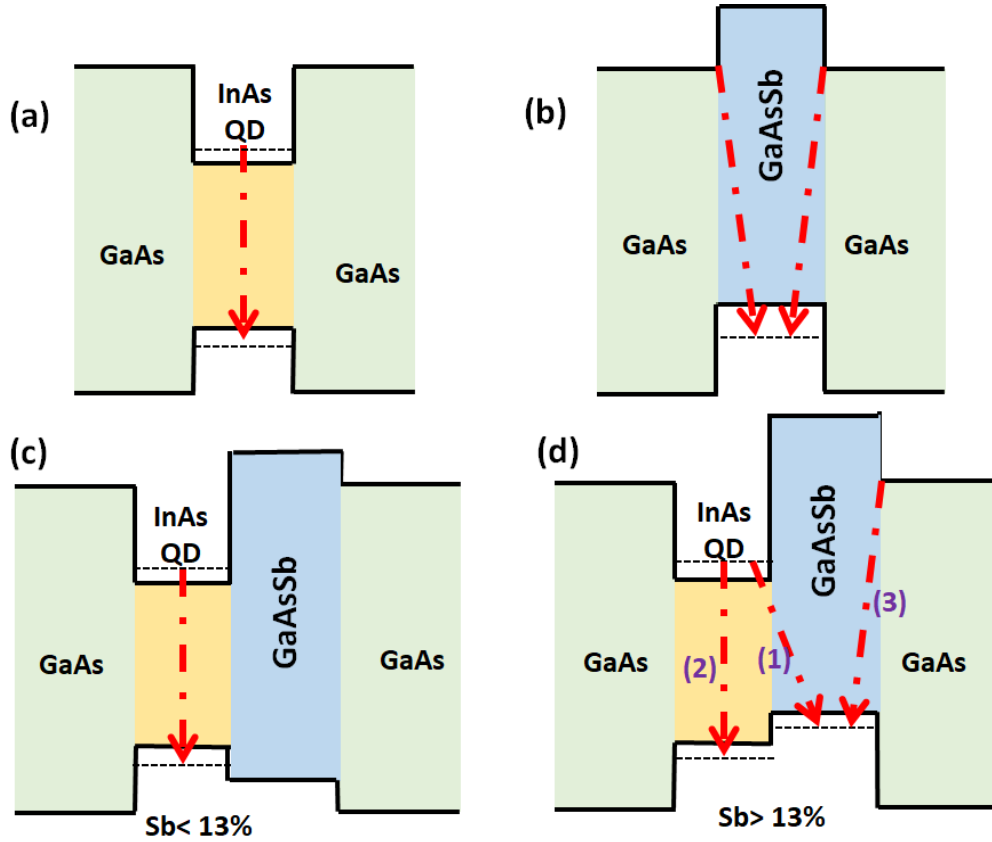


Fig. 16 Schematic diagram of band structures. (a) InAs/GaAs QDs. (b) GaAs/GaAsSb QW. (c) InAs/ $\text{GaAs}_{1-x}\text{Sb}_x$ when $x < 0.13$. (d) InAs/ $\text{GaAs}_{1-x}\text{Sb}_x$ when $x > 0.13$.

To further confirm the type-I to type-II transition, power-dependent PL measurements were performed at 7K, with the excitation energies varying from 100mW to 0.001mW. For type-I band alignment, the PL peak position should be independent of excitation power, while a linear relationship between PL peak energy and the cube root of the excitation power is a symbol of a type-II band alignment [29]. The power-dependent PL spectra for InAs/GaAs QDs and GaAs/GaAsSb QW structures are shown in Figs. 17(a) and (b), correspondingly. The PL peak

from the ground states of InAs quantum dots shows a type-I band alignment nature since the peak energy is independent of the excitation power. The other PL peak from the first excited QDs state only appears at high excitation energy, still type-I. In contrast, the quantum well structure shows a type-II behavior, which demonstrated by the linear relationship between the cube root of the excitation energy and peak energy. With a small portion of Sb added in the capping layer, as shown in Fig. 17 (c) (Sb=11%), the better uniformity of quantum dots can be determined as the peak shows less shift comparing with InAs/GaAs QDs, and it also consistent with the AFM evaluation results.

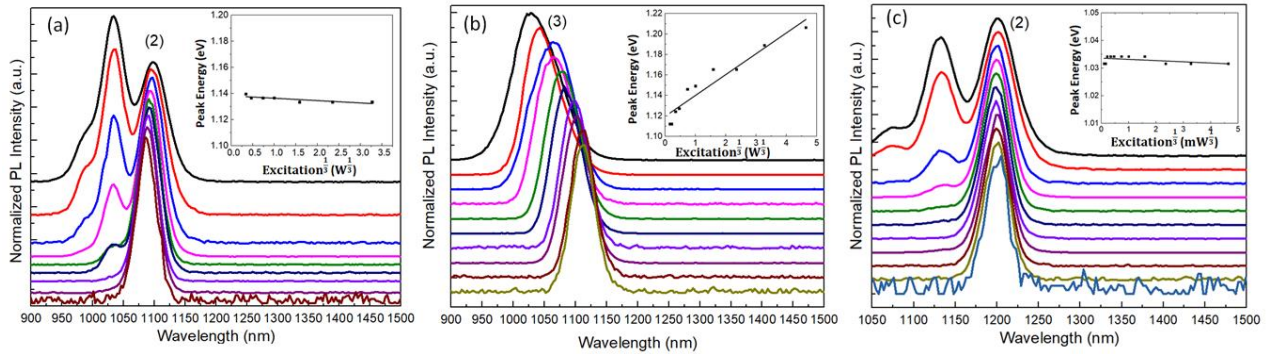


Fig. 17 Power-dependent PL at 7K from (a) InAs/GaAs QDs, (b) GaAs/GaAsSb QWs, and (c) InAs/GaAs_{1-x}Sb_x QDs with x=0.11.

As illustrated earlier in Fig. 16, when the Sb composition exceeds 13%, more recombination routes will take place. Here, we measured InAs/GaAs_{1-x}Sb_x QDs with Sb=25% as an example. In Fig. 18 (a), PL peaks (1), (2) and (3) are labeled corresponding to the three recombination routes depicted in Fig. 16 (d). This result is different from previous study which shows two peaks when Sb=15% and 25% [30]. These peaks exhibit different responses to the excitation energies. At low excitation energy, the recombination firstly occurs between conduction band of QDs and valence band of GaAsSb spacer. PL peak (1) around 1290 nm is observed with a type-II alignment, proved by the inset of Fig. 18 (a). As the excitation intensity rises higher, peak

(2) located around 1180 nm appears with a type-I alignment, proved by Fig. 18 (b), as the peak position has little change with excitation intensity. The peak (2) thus comes from carrier recombination inside the InAs QDs. By comparing peak (2) in Fig. 18 (a) and Fig. 17 (a), the reduced PL energy and intensity can be attributed to the strain reduction with GaAsSb capping layer and the carrier transfer effect from GaAsSb spacer, respectively. When the excitation intensity increases higher, peak (3) appears at ~1050 nm with a type-II band structure under GaAs/GaAsSb QW, shown in Fig. 18 (b). The PL at high excitation power in Fig. 17 (b) shows a similar peak position with peak (3) in Fig. 18 (a).

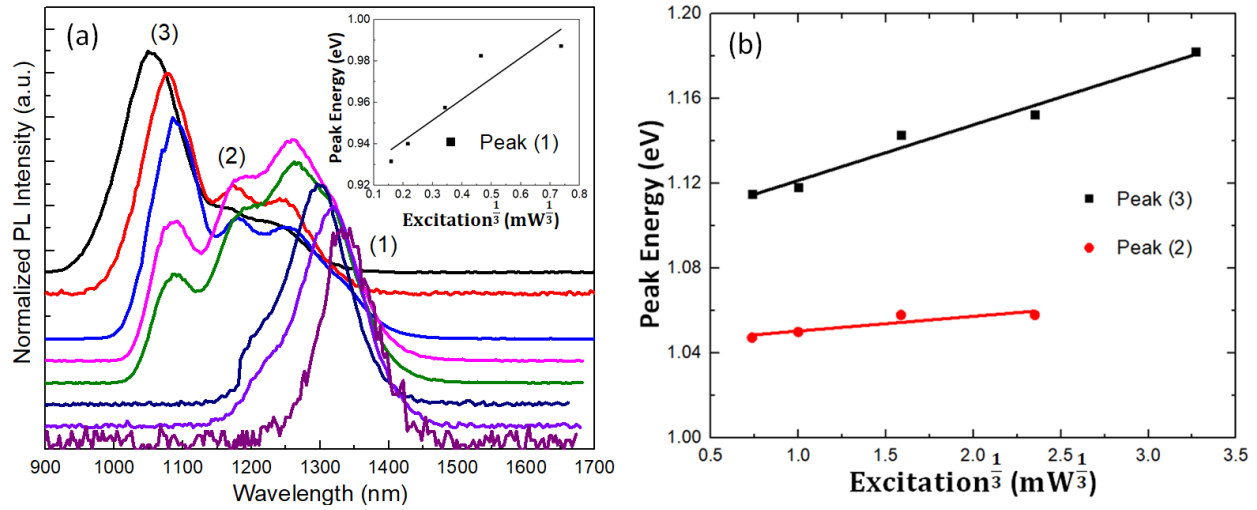


Fig. 18 (a) Power-dependent PL at 7K from GaAs_{1-x}Sb_x QDs with x=0.25, the inset shows the linear relationship between the peak (1) energy versus the cube root of excitation energy. (b) PL peak energy versus the cube root of the excitation energy for peak (3) and (2).

TRPL measurements are performed to understand the type-I and type-II alignment in more detail. A NKT super-continuum laser with wavelength of 532 nm, ~20ps pulse width and 7.8 MHz repetition rate, is used to excited the samples. An infrared-enhanced photodetector along with PicoHarp 300 Time-Correlated Single Photon Counting (TCSPC) system is used for photon

detection. The decay curves are taken for InAs/GaAs QDs, GaAs/GaAsSb QWs, InAs/ GaAs_{1-x}Sb_x QDs with Sb=15% and Sb=25% at 7K, shown in Fig. 19 respectively.

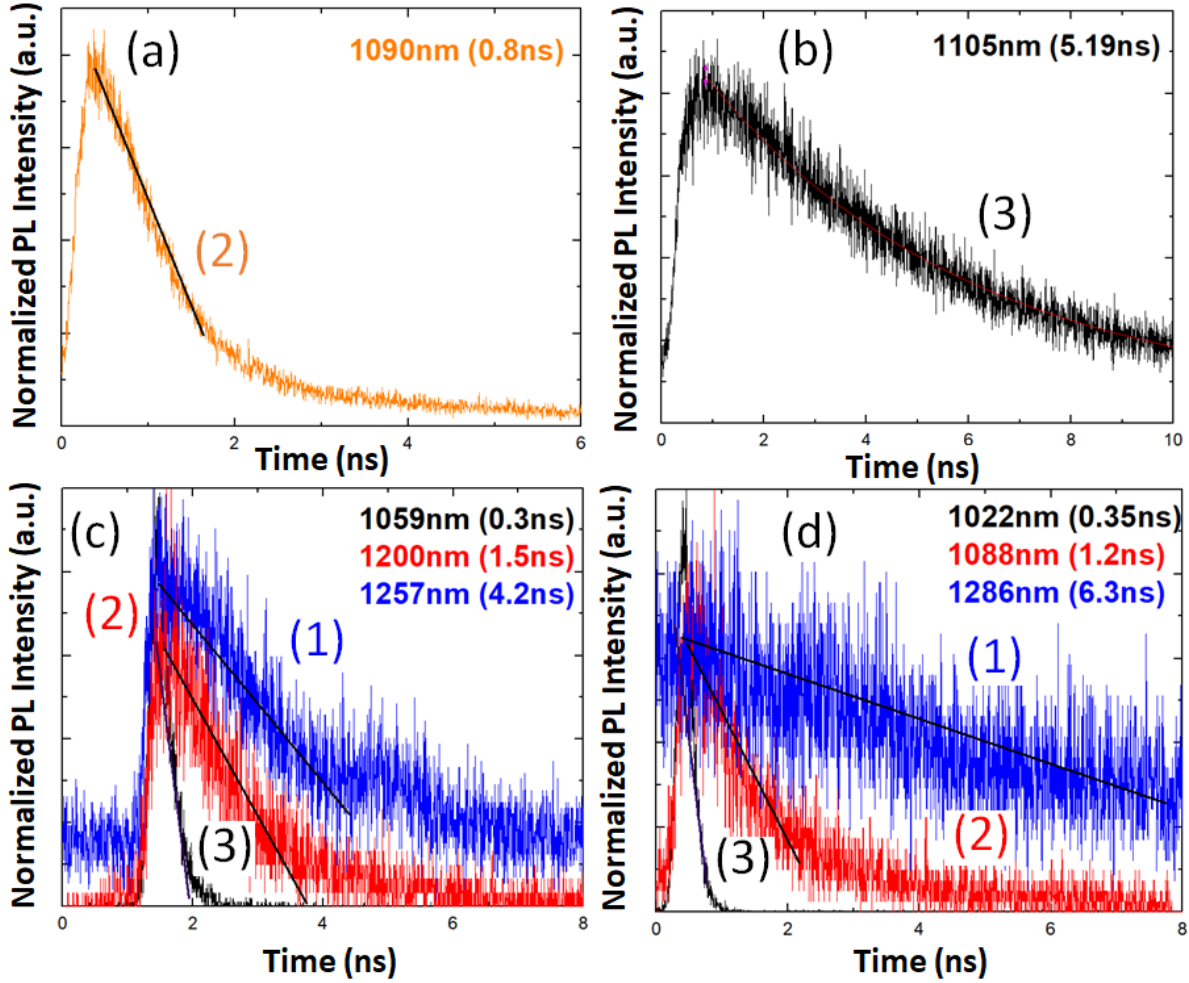


Fig. 19 TRPL decay curves measured at 7K for (a) InAs/GaAs QDs, (b) GaAs/GaAsSb QWs, (c) InAs/ GaAs_{1-x}Sb_x QDs with Sb=15% and (d) Sb=25%. Black lines are fits with single exponential decay functions.

The lifetimes of InAs/GaAs QDs and GaAs/GaAsSb QWs are firstly measured as shown in Fig. 19 (a) and 19 (b). The measured lifetime for the InAs quantum dots is 0.8ns, agrees with the previous study [31]. The lifetime of carriers from the type-II quantum well is 5.19 ns, much longer than those from the quantum dots, also have been proved [32]. For InAs/ GaAs_{1-x}Sb_x QDs

with Sb=15% and Sb=25%, peak (1), (2) and (3) are correspond with the three routes of carrier recombination. Peak (1) in Fig. 19 (c) and 19 (d) are originated from the type-II recombination of electrons in InAs QDs and holes in GaAsSb spacer, show a relatively long lifetime of 4.2 ns and 6.3 ns [33]. Peak (2) in Fig. 19 (c) and 19 (d) are emitted from the InAs QDs, have a longer lifetime of 1.5 ns and 1.2 ns, comparing with 0.8 ns in Fig. 19 (a). The longer lifetime may due to the effect of GaAsSb layer next to the QD layer, causing a pseudo- type-II transition. Peak (3) in Fig. 19 (c) and 19 (d) show a dramatic drop of the lifetime of 0.3 ns and 0.35 ns, comparing with Fig. 19 (b). The strong carrier transfer competition between QDs and GaAsSb layer may decrease the lifetime of peak (3).

5. Conclusion

In this work, the self-assembled quantum dots growth process and the MBE growth technology are reviewed. Later, the structural and optical characterization methods, including AFM, XRD, TEM and PL, are reviewed. The IBSC concept is realized by the SAQDs structure and InAs QDs structure is proposed to capped by GaAsSb layer. With different composition of Sb, InAs/ GaAs_{1-x}Sb_x QDs shows a strain reduction at low Sb concentration and exhibits a type-I to type-II band alignment transition.

InAs/ GaAs_{1-x}Sb_x QDs samples with different Sb composition are grown and compared. AFM is used to evaluate quantum dots qualities of QDs on the GaAsSb buffer layer under different QD layer thickness and Sb concentrations. It can be concluded that Sb =12% with 3ML of QD layer thickness provides better quantum dots qualities based on comparison. The optical characterization is studied in detail based on time-integrated PL and TRPL. The PL peak energies are compared and type-I and type-II band alignment properties are revealed by power-dependent PL measurements. InAs/GaAs QDs sample shows a type-I band alignment while GaAs/GaAsSb QWs structure shows a type-II alignment. At low Sb concentration (Sb<13%), InAs/ GaAs_{1-x}Sb_x QDs sample is still type-I, and GaAsSb spacer acts as strain compensation layer mostly, which enhances the quality of quantum dots. At high Sb concentration (Sb>13%), InAs/ GaAs_{1-x}Sb_x QDs shows a degradation of quantum dots, indicated by the spectra broadening. Also, PL peaks with type-II properties appear, suppressing carrier recombination inside the QDs. TRPL data show a longer lifetime of carriers from type-II structures, which shows the high potential of InAs/ GaAs_{1-x}Sb_x QDs for SAQDs in the application of IBSC.

REFERENCES

- [1] Shockley, W., & Queisser, H. J. (1961). Detailed balance limit of efficiency of p-n junction solar cells. *Journal of applied physics*, 32(3), 510-519.
- [2] Schaller, Richard D., and Victor I. Klimov. "High efficiency carrier multiplication in PbSe nanocrystals: implications for solar energy conversion." *Physical review letters* 92.18 (2004): 186601.
- [3] Ross, Robert T., and Arthur J. Nozik. "Efficiency of hot-carrier solar energy converters." *Journal of Applied Physics* 53.5 (1982): 3813-3818.
- [4] Guter, Wolfgang, et al. "Current-matched triple-junction solar cell reaching 41.1% conversion efficiency under concentrated sunlight." *Applied Physics Letters* 94.22 (2009): 223504.
- [5] Luque, Antonio, and Antonio Martí. "Increasing the efficiency of ideal solar cells by photon induced transitions at intermediate levels." *Physical Review Letters* 78.26 (1997): 5014.
- [6] Im, J. H., Lee, C. R., Lee, J. W., Park, S. W., & Park, N. G. (2011). 6.5% efficient perovskite quantum-dot-sensitized solar cell. *Nanoscale*, 3(10), 4088-4093.
- [7] Ohring, Milton. *Materials science of thin films*. Elsevier, 2001.
- [8] J. M. Moison, F. Houzay, F. Barthe, L. Leprince, E. André, and O. Vatel, "Selforganized growth of regular nanometer-scale InAs dots on GaAs," *Appl. Phys. Lett.*, vol. 64, p. 196, 1994.
- [9] Gonzalez, D., et al. "Influence of Sb/N contents during the capping process on the morphology of InAs/GaAs quantum dots." *Solar Energy Materials and Solar Cells* 145 (2016): 154-161.
- [10] Franchi, S., et al. "Quantum dot nanostructures and molecular beam epitaxy." *Progress in Crystal Growth and Characterization of Materials* 47.2 (2003): 166-195.
- [11] A.Y. Cho. in: E.H.C. Parker (Ed.), *The technology and physics of molecular beam epitaxy*, vol. 1, Plenum Press, New York, NY, 1985.
- [12] Heyn, Ch. "Critical coverage for strain-induced formation of InAs quantum dots." *Physical Review B* 64.16 (2001): 165306.
- [13] Guimard, Denis, et al. "Fabrication of InAs/GaAs quantum dot solar cells with enhanced photocurrent and without degradation of open circuit voltage." *Applied Physics Letters* 96.20 (2010): 203507.
- [14] Hubbard, S. M., et al. "Effect of strain compensation on quantum dot enhanced GaAs solar cells." *Applied Physics Letters* 92.12 (2008): 123512.
- [15] Utrilla, A. D., et al. "Thin GaAsSb capping layers for improved performance of InAs/GaAs quantum dot solar cells." *Solar Energy Materials and Solar Cells* 159 (2017): 282-289.
- [16] Liu, Wei-Sheng, et al. "High optical property vertically aligned InAs quantum dot structures with GaAsSb overgrown layers." *Journal of Crystal Growth* 323.1 (2011): 164-166.

- [17] W. S. Liu, Y. T. Wang, W. Y. Qiu, and C. Fang, "Carrier dynamics of a type-II vertically aligned InAs quantum dot structure with a GaAsSb strain-reducing layer," *Appl. Phys. Express* 6(8), 085001 (2013).
- [18] H. Liu, M. J. Steer, T. J. Badcock, D. J. Mowbray, M. S. Skolnick, P. Navaretti, K. M. Groom, M. Hopkinson, and R. A. Hogg, "Long-wavelength light emission and lasing from InAs/GaAs quantum dots covered by a GaAsSb strain-reducing layer," *Appl. Phys. Lett.* 86(14), 143108 (2005).
- [19] Zeng, Guanghong, et al. "Nanomechanics of Amyloid Materials Studied by Atomic Force Microscopy." *Atomic Force Microscopy Investigations into Biology-From Cell to Protein*. InTech, 2012.
- [20] Oshima, Ryuji, Ayami Takata, and Yoshitaka Okada. "Strain-compensated InAs/GaNAs quantum dots for use in high-efficiency solar cells." *Applied Physics Letters* 93.8 (2008): 083111.
- [21] Ustinov, V. M., et al. "InAs/InGaAs quantum dot structures on GaAs substrates emitting at 1.3 μm ." *Applied physics letters* 74.19 (1999): 2815-2817.
- [22] Li, Aigen. "Interaction of nanoparticles with radiation." arXiv preprint astro-ph/0311066 (2003).
- [23] Debnath, M. C., et al. "High-density InAs/GaAs $_{1-x}$ Sb $_x$ quantum-dot structures grown by molecular beam epitaxy for use in intermediate band solar cells." *Journal of Applied Physics* 119.11 (2016): 114301.
- [24] Ponchet, A., et al. "Elastic energy of strained islands: Contribution of the substrate as a function of the island aspect ratio and inter-island distance." *Applied physics letters* 72.23 (1998): 2984-2986.
- [25] Ulloa, J. M., et al. "GaAsSb-capped InAs quantum dots: from enlarged quantum dot height to alloy fluctuations." *Physical Review B* 81.16 (2010): 165305.
- [26] He, Jun, Feng Bao, and Jinping Zhang. "Capping effect of GaAsSb and InGaAsSb on the structural and optical properties of type II GaSb/GaAs quantum dots." *Applied Physics Letters* 100.17 (2012): 171914.
- [27] Guo, Yingnan, et al. "Carrier dynamics of InAs quantum dots with GaAs $_{1-x}$ Sb $_x$ barrier layers." *Applied Physics Letters* 111.19 (2017): 191105.
- [28] Cheng, Y., et al. "Investigation of InAs/GaAs $_{1-x}$ Sb $_x$ quantum dots for applications in intermediate band solar cells." *Solar Energy Materials and Solar Cells* 147 (2016): 94-100.
- [29] Chiu, Y. S., et al. "Properties of photoluminescence in type-II GaAsSb/GaAs multiple quantum wells." *Journal of applied physics* 92.10 (2002): 5810-5813.
- [30] Zíková, Markéta, et al. "Comparison of MOVPE grown GaAs, InGaAs and GaAsSb covering layers for different InAs/GaAs quantum dot applications." *Journal of Crystal Growth* 464 (2017): 59-63.
- [31] He, J., et al. "Band Alignment Tailoring of InAs $_{1-x}$ Sb $_x$ /GaAs Quantum Dots: Control of Type I to Type II Transition." *Nano letters* 10.8 (2010): 3052-3056.

- [32] Luo, X. D., et al. "Selectively excited photoluminescence of GaAs $1-x$ Sb x /GaAs single quantum wells." *Applied physics letters* 81.20 (2002): 3795-3797.
- [33] Chen, T. T., et al. "Unusual optical properties of type-II In As/Ga As 0.7 Sb 0.3 quantum dots by photoluminescence studies." *Physical Review B* 75.3 (2007): 033310.
- [34] Moison, J. M., et al. "Self-organized growth of regular nanometer-scale InAs dots on GaAs." *Applied Physics Letters* 64.2 (1994): 196-198.